

Dear Author,

Here are the proofs of your article.

- You can submit your corrections **online**, via **e-mail** or by **fax**.
- For **online** submission please insert your corrections in the online correction form. Always indicate the line number to which the correction refers.
- You can also insert your corrections in the proof PDF and **email** the annotated PDF.
- For fax submission, please ensure that your corrections are clearly legible. Use a fine black pen and write the correction in the margin, not too close to the edge of the page.
- Remember to note the **journal title**, **article number**, and **your name** when sending your response via e-mail or fax.
- **Check** the metadata sheet to make sure that the header information, especially author names and the corresponding affiliations are correctly shown.
- **Check** the questions that may have arisen during copy editing and insert your answers/ corrections.
- **Check** that the text is complete and that all figures, tables and their legends are included. Also check the accuracy of special characters, equations, and electronic supplementary material if applicable. If necessary refer to the *Edited manuscript*.
- The publication of inaccurate data such as dosages and units can have serious consequences. Please take particular care that all such details are correct.
- Please **do not** make changes that involve only matters of style. We have generally introduced forms that follow the journal's style. Substantial changes in content, e.g., new results, corrected values, title and authorship are not allowed without the approval of the responsible editor. In such a case, please contact the Editorial Office and return his/her consent together with the proof.
- If we do not receive your corrections **within 48 hours**, we will send you a reminder.
- Your article will be published **Online First** approximately one week after receipt of your corrected proofs. This is the **official first publication** citable with the DOI. **Further changes are, therefore, not possible.**
- The **printed version** will follow in a forthcoming issue.

Please note

After online publication, subscribers (personal/institutional) to this journal will have access to the complete article via the DOI using the URL: [http://dx.doi.org/\[DOI\]](http://dx.doi.org/[DOI]).

If you would like to know when your article has been published online, take advantage of our free alert service. For registration and further information go to: <http://www.link.springer.com>.

Due to the electronic nature of the procedure, the manuscript and the original figures will only be returned to you on special request. When you return your corrections, please inform us if you would like to have these documents returned.

Metadata of the article that will be visualized in OnlineFirst

Please note: Images will appear in color online but will be printed in black and white.

ArticleTitle	Modelling of an Atmospheric Pressure Nitrogen Glow Discharge Operating in High-Gas Temperature Regimes
--------------	--

Article Sub-Title

Article CopyRight	Springer Science+Business Media New York (This will be the copyright line in the final PDF)
-------------------	--

Journal Name	Plasma Chemistry and Plasma Processing
--------------	--

Corresponding Author	Family Name	Prevosto
	Particle	
	Given Name	L.
	Suffix	
	Division	Grupo de Descargas Eléctricas, Departamento Ing. Electromecánica
	Organization	Facultad Regional Venado Tuerto (UTN)
	Address	Laprida 651, 2600, Venado Tuerto, Santa Fe, Argentina
	Email	prevosto@waycom.com.ar
	ORCID	

Author	Family Name	Kelly
	Particle	
	Given Name	H.
	Suffix	
	Division	Grupo de Descargas Eléctricas, Departamento Ing. Electromecánica
	Organization	Facultad Regional Venado Tuerto (UTN)
	Address	Laprida 651, 2600, Venado Tuerto, Santa Fe, Argentina
	Division	Instituto de Física del Plasma (CONICET)
	Organization	Facultad de Ciencias Exactas y Naturales (UBA) Ciudad Universitaria Pab. I
	Address	1428, Buenos Aires, Argentina
	Email	
	ORCID	

Author	Family Name	Mancinelli
	Particle	
	Given Name	B.
	Suffix	
	Division	Grupo de Descargas Eléctricas, Departamento Ing. Electromecánica
	Organization	Facultad Regional Venado Tuerto (UTN)
	Address	Laprida 651, 2600, Venado Tuerto, Santa Fe, Argentina
	Email	
	ORCID	

Schedule	Received	6 April 2016
	Revised	

Abstract

A model of an atmospheric pressure nitrogen glow discharge in high-gas temperature regimes is developed. The model considers a fairly complete set of chemical reactions, including several processes with the participation of electronically excited nitrogen atoms describing the energy balance and charged particles kinetic processes in the discharge. It is shown that the thermal dissociation of vibrationally excited molecules plays an essential role in the production of $N(^4S)$ atoms. The dominant ion within the investigated current range (52–187 mA) is the molecular N_2^+ with an increasing proportion of atomic N^+ towards high-current values. The process of production of electrons within the almost whole current range is controlled predominantly by associative ionization in atomic collisions $N(^2P) + N(^2P) \rightarrow N_2^+ + e$; being the $N(^2P)$ atoms mainly produced via quenching of $N_2(A^3\Sigma_u^+)$ electronically excited molecules by $N(^4S)$ atoms. The results of calculations are compared with the available experimental data and a good agreement is found.

Keywords (separated by '-') Glow discharge - Nitrogen gas - Electronic metastable atoms - Atmospheric pressure

Footnote Information



Modelling of an Atmospheric Pressure Nitrogen Glow Discharge Operating in High-Gas Temperature Regimes

L. Prevosto¹ · H. Kelly^{1,2} · B. Mancinelli¹Received: 6 April 2016 / Accepted: 4 May 2016
© Springer Science+Business Media New York 2016

Abstract A model of an atmospheric pressure nitrogen glow discharge in high-gas temperature regimes is developed. The model considers a fairly complete set of chemical reactions, including several processes with the participation of electronically excited nitrogen atoms describing the energy balance and charged particles kinetic processes in the discharge. It is shown that the thermal dissociation of vibrationally excited molecules plays an essential role in the production of $N(^4S)$ atoms. The dominant ion within the investigated current range (52–187 mA) is the molecular N_2^+ with an increasing proportion of atomic N^+ towards high-current values. The process of production of electrons within the almost whole current range is controlled predominantly by associative ionization in atomic collisions $N(^2P) + N(^2P) \rightarrow N_2^+ + e$; being the $N(^2P)$ atoms mainly produced via quenching of $N_2(A^3\Sigma_u^+)$ electronically excited molecules by $N(^4S)$ atoms. The results of calculations are compared with the available experimental data and a good agreement is found.

Keywords Glow discharge · Nitrogen gas · Electronic metastable atoms · Atmospheric pressure

Introduction

Atmospheric pressure glow discharges are of interest as plasma sources for a number of technological applications, including plasma decontamination and sterilization, biomedical applications, material processing, modification of electromagnetic waves propagation, and

A1 L. Prevosto
A2 prevosto@waycom.com.ar

A3 ¹ Grupo de Descargas Eléctricas, Departamento Ing. Electromecánica, Facultad Regional Venado
A4 Tuerto (UTN), Laprida 651, 2600 Venado Tuerto, Santa Fe, Argentina

A5 ² Instituto de Física del Plasma (CONICET), Facultad de Ciencias Exactas y Naturales (UBA)
A6 Ciudad Universitaria Pab. I, 1428 Buenos Aires, Argentina



27 plasma aerodynamics [1–3]. The glow discharge is normally obtained at low-gas pressures,
28 but it can be maintained in a similar form if the pressure is increased up to and above the
29 atmospheric value [2–11]. The experimental data show that both low and high-pressure
30 glow discharges are characterized by a non-equilibrium distribution of energy among the
31 different degrees of freedom of the plasma species [5–10]. Usually each energy distribution
32 can be described by a characteristic temperature; such as the electron temperature (T_e),
33 vibrational temperature (T_v), rotational temperature (T_r), and translational (gas) tempera-
34 ture (T_g). In non-equilibrium plasmas created by externally applied electric fields, typically
35 $T_e > T_v > T_r = T_g$ [6–8]. The non-equilibrium state allows for the creation of active
36 species without generating excessive heat. However, at pressure levels of the order of the
37 atmospheric value, a strong non-equilibrium plasma state is hardly to maintain due to the
38 thermalization of the discharge, which leads to a sudden (or continuous [4]) transition from
39 the glow to the arc phase [12–15]; being the final stage closer to the thermodynamic
40 equilibrium. The transition is characterized by an increase in the current density and a
41 considerable fall in the discharge voltage (due to the switching of secondary electron
42 emission to thermionic emission of electrons from the cathode surface).

43 The discharge thermalization typically arises due to the so called thermal instability [12,
44 16], which results in a rapid increase in the gas temperature. Generally, the thermal
45 instability can be prevented if the gas residence time in the discharge is small compared
46 with the heating time (which is determined by the rate of energy transfer from the electrons
47 to the translational degree of freedom of the heavy particles). In atomic gases the main
48 mechanism of gas heating is by elastic collisions. For reduced electric fields $E/N > 30$ Td
49 (where E is the electric field strength, N the gas number density and $1 \text{ Td} \equiv 10^{-21} \text{ V m}^2$),
50 the fractional electron power transferred in elastic collisions to gas heating is less than a
51 few times 10^{-3} [17]. In molecular gases, however, electrons can transfer energy to internal
52 energy states of the molecule, such as the vibrational mode. Since for $30 < E/N < 50$ Td
53 the typical electron temperatures in molecular gases (of about 1 eV) are comparable to the
54 characteristic vibrational energy values (0.2–0.5 eV) of the molecules, most of the electron
55 energy (~ 80 to 98 %) is transferred to vibrational modes, and then partially to gas heating,
56 mainly through the mechanism of vibrational–translational (V–T) relaxation [17, 18]. As
57 inelastic losses are usually greater than elastic ones by one to two orders of magnitude [16],
58 molecular gases typically have higher heating rates and are more susceptible to thermal-
59 ization than atomic gases. This is due to the strong exponential dependence of the V–T
60 relaxation rate coefficient on the gas temperature. Even small increases of the gas temper-
61 ature lead to a significant increase of the V–T relaxation rate, intensification of heating,
62 and then to a further growth of the gas temperature. This process takes typically a relatively
63 long time ($\sim 100 \mu\text{s}$) in nitrogen gas at atmospheric pressure [18].

64 In direct-current (dc) glow discharges at atmospheric pressure, high-speed gas flows
65 have been used to provide sufficient cooling of discharges at high pressures [19, 20]. If the
66 gas residence time in the discharge is small as compared with the V–T relaxation time, the
67 gas heating is almost suppressed and the molecular gas is in a strongly non-equilibrium
68 state. This state is characterized by a level of vibrational energy that considerable exceeds
69 its equilibrium value. On the other hand, for discharge conditions such that the gas resi-
70 dence time in the discharge is larger than the V–T relaxation time (e.g., still discharges),
71 the molecular gas changes to a state close to the thermodynamically equilibrium one, with
72 a higher gas temperature as in an arc discharge.

73 In [21], experimental information on the properties of the atmospheric pressure con-
74 stricted discharge in a longitudinal nitrogen flow was published. A steady-state pin-to-
75 plane glow discharge was generated inside a tube where a flow of nitrogen was injected up



76 to a velocity of 20 m/s. The inter-electrode gap was 15 mm. The results showed that the
77 gas flow rate has a strong influence on the properties of the discharge.

78 In [22, 23], atmospheric pressure glow discharges in a fast longitudinal flow of air and
79 nitrogen plasmas were investigated. The nitrogen gas was preheated up to 1800–2250 K
80 and then was injected through a nozzle in the discharge region at a velocity of about
81 450 m/s. A glow discharge was ignited between two needle electrodes oriented along the
82 axis of the gas stream, and separated a distance of 3.5 cm. The discharge current was
83 $I < 250$ mA. Owing to the fast gas flow rate the gas temperature remained practically
84 constant in the discharge region.

85 In [24], an atmospheric pressure glow discharge in a slow longitudinal flow of nitrogen
86 plasma was investigated. Nitrogen was injected through a flow straightener and passed
87 through the discharge region with a velocity of only 20 cm/s. The glow discharge was
88 formed between a pair of platinum pins (separation 0.85 cm) that were vertically mounted
89 along the axis of the gas stream. The discharge was maintained by a dc power supply
90 ($I < 250$ mA) in a ballasted circuit. The radial profile of the N_2^+ concentration and the
91 values of the gas rotational temperature were experimentally inferred for currents $I = 52$,
92 97, 142 and 187 mA. Peak (centerline) density values around 10^{18} m^{-3} and high-rotational
93 temperature values (obtained from Boltzmann plots), ranging from 3100 to 4700 K, were
94 measured in the given current range.

95 In contrast to the relatively large number of works devoted to the experimental char-
96 acterization (mainly spectral and electrical characteristics of constricted discharges) of
97 atmospheric pressure glow discharges in nitrogen (with flowing gas and with still gas) [2–
98 11, 21–24], there are only few published investigations on the energy balance and charged
99 particles kinetics relevant to the sustaining of the non-equilibrium state.

100 In [25], a one-dimensional model of a dc glow discharge with variable nitrogen flow
101 rates (velocities up to 20 m/s) at atmospheric pressure for a low-current regime
102 ($I = 5$ mA) and for a high-current regime ($I = 40$ mA); was presented. The results
103 showed that the charged particle generation in both current regimes was mainly controlled
104 by associative ionization involving molecular metastable states, although marked differ-
105 ences in the calculated plasma composition were found. For $I = 5$ mA the dominant ion
106 was N_3^+ while for $I = 40$ mA was N^+ . Owing to the extremely low value of the
107 recombination coefficient for atomic ions, the dynamic balance of the charged particles
108 was non-local (with a large diffusion of the atomic ions) for the larger current value, while
109 for the lower current value was local (volume electron-ion recombination). However, it
110 should be noted that the calculated composition for $I = 40$ mA was not consistent with the
111 measured results [24]; which indicated that the dominant ion under similar plasma con-
112 ditions was the molecular one. In [26], another model for non-equilibrium nitrogen plas-
113 mas was presented. The rate constants of reactions involving electrons were obtained by
114 averaging the corresponding cross sections with the Maxwellian electron energy distri-
115 bution function (EEDF). The obtained results suggested that the vibrational temperature
116 was well approximated by the gas temperature at low electron number densities and by the
117 electron temperature at high electron number densities (thus indicating that the plasma
118 switches from a regime where the vibrational levels are mainly equilibrated by collisions
119 with heavy particles to another regime where they are equilibrated by collisions with
120 electrons). In [27], a simplified chemical kinetic model of a slightly-ionized atmospheric
121 pressure nitrogen discharge was given. No energy balance equation was used and the



122 temperature of the species was imposed. The model was tested against calculations of
 123 Saha–Boltzmann equilibrium state, and a reasonable good agreement was achieved. It was
 124 found that in equilibrium conditions the electrons are produced by associative ionization
 125 involving atoms.

126 In this work, a model of an atmospheric pressure nitrogen glow discharge in high-gas
 127 temperature regimes (simulating the conditions of [24]) is proposed. The model includes a
 128 fairly complete set of chemical reactions and describes the processes of the energy balance
 129 and charged particles kinetic processes governing the discharge. The major difference
 130 between the model [25] and that used in this work is the inclusion of several processes with
 131 the participation of electronically excited nitrogen atoms. The results of calculations are
 132 compared with the available experimental data [24] and a good agreement is found.

133 The Model

134 The model includes the continuity equations for the most important neutral and charged
 135 species present in the nitrogen discharge together with the balance equations describing the
 136 mean-vibrational energy of the nitrogen molecules and the gas kinetic energy. The
 137 numerical calculations were done under the assumption that $p = 1$ atm, (where p is the gas
 138 pressure). The considered species for pure nitrogen are the vibrational manifold of ground
 139 state molecules $N_2(X^1\Sigma_g^+, v)$, the electronic excited states of nitrogen molecules
 140 $N_2(A^3\Sigma_u^+)$, $N_2(B^3\Pi_g)$, $N_2(a^1\Sigma_u^-)$ and $N_2(C^3\Pi_u)$, the electronic excited states of nitrogen
 141 atoms, $N(^2D)$ and $N(^2P)$, the atomic ground state $N(^4S)$, the positive ions N_4^+ , N_3^+ , N_2^+
 142 and N^+ ; and the electrons (e). The continuity equations for the active species were solved
 143 for the densities of $N_2(A^3\Sigma_u^+)$, $N_2(B^3\Pi_g)$, $N_2(a^1\Sigma_u^-)$, $N_2(C^3\Pi_u)$, $N(^2D)$, $N(^2P)$, $N(^4S)$,
 144 N_4^+ , N_3^+ , N^+ and electrons. The density of the dominating sort of positive ions N_2^+ , was
 145 obtained from the condition of charge conservation (the electrodes sheaths were not
 146 included in the calculations) while the density of the dominant species $N_2(X^1\Sigma_g^+, v)$ was
 147 obtained from the constancy of the pressure. The continuity equations for the plasma
 148 particles were solved in a local approximation

$$\frac{\partial}{\partial t}(Y_i) = \sum_j S_{ij}, \quad (1)$$

150 where Y_i is the number density and S_{ij} is the rate of production of the i th species in the j th
 151 reaction (negative if the species is destroyed). In high-pressure plasmas this approximation
 152 is usually justified by the long time scale for diffusive losses (inversely proportional to the
 153 collision rate) compared with the relatively short time scale to achieve local equilibrium
 154 (proportional to the collision rate) [16]. The time scales for diffusive losses for charged and
 155 neutral particles may be estimated as R^2/D_{ea} and R^2/D ; where R is the radius of the
 156 discharge column, D_{ea} is the coefficient of ambipolar diffusion of electrons in the presence
 157 of multiple ions, and D is the coefficient of diffusion of neutral species. The ambipolar
 158 diffusion D_{ea} can be estimated in a simplified fashion in terms of the mobility μ_p of N_2^+
 159 only, the dominating sort of positive ions in nitrogen under the considered conditions.
 160 According to [28], $\mu_p = 4.51 \times 10^{21}/N \text{ m}^2/\text{V s}$. For $T_g \sim 4000$ K and $T_e \sim 9000$ K, it
 161 results $D_{ea} \sim 2.8 \times 10^{-3} \text{ m}^2/\text{s}$. The neutral diffusion coefficient D can be estimated for
 162 the $N(^2P)$ atoms as $D = 0.185 \times 10^{-4} (T_g/273)^{3/2} \text{ m}^2/\text{s}$ [18]. For the gas temperature

Table 1 Plasma processes (Ri) and their rate coefficients and applicable references

No.	Reaction	Rate coefficient [m ³ /s or m ⁶ /s (*)]	References
<i>Electron-impact excitation</i>			
(R1)	$e + N_2(X) \rightarrow e + N_2(X, \text{Elastic})$	k is a function of $f(E/N)$	[35]
(R2)	$e + N_2(X) \rightarrow e + N_2(X, \text{Rot})$	k is a function of $f(E/N)$ Threshold energy = 0.02 eV	[35]
(R3)	$e + N_2(X, v) \rightarrow e + N_2(A)$	k is a function of $f(E/N, T_v)$	[35]
(R4)	$e + N_2(X, v) \rightarrow e + N_2(B)$	k is a function of $f(E/N, T_v)$	[35]
(R5)	$e + N_2(X, v) \rightarrow e + N_2(a')$	k is a function of $f(E/N, T_v)$	[35]
(R6)	$e + N_2(X, v) \rightarrow e + N_2(C)$	k is a function of $f(E/N, T_v)$	[35]
<i>Electron-impact dissociation</i>			
(R7)	$e + N_2(X, v) \rightarrow N_2(E^* = 13 \text{ eV})$ $N_2(E^* = 13 \text{ eV}) \rightarrow N(^4S) + N(^2D)$	k is a function of $f(E/N, T_v)$	[35]
<i>Direct electron-impact ionization</i>			
(R8)	$e + N_2(X, v) \rightarrow e + e + N_2^+$	k is a function of $f(E/N, T_v)$	[35]
<i>Stepwise ionization</i>			
(R9)	$e + N_2(A) \rightarrow e + e + N_2^+$	Calculated from the cross section data of [44]. k is a function of $f(E/N, T_v)$	[35, 44]
(R10)	$e + N_2(B) \rightarrow e + e + N_2^+$	Calculated from the cross section data of [44]. k is a function of $f(E/N, T_v)$	[35, 44]
(R11)	$e + N_2(a') \rightarrow e + e + N_2^+$	Calculated from the cross section data of [44]. k is a function of $f(E/N, T_v)$	[35, 44]
<i>Penning/associative ionization</i>			
(R12)	$N_2(A) + N_2(a') \rightarrow e + N_4^+$	$0.5 \times 5.0 \times 10^{-17}$	[32, 33, 53]
(R13)	$N_2(A) + N_2(a') \rightarrow e + N_2(X) + N_2^+$	$0.5 \times 5.0 \times 10^{-17}$	[32, 33, 53]
(R14)	$N_2(a') + N_2(a') \rightarrow e + N_4^+$	$0.5 \times 2.0 \times 10^{-16}$	[32, 33, 53]
(R15)	$N_2(a') + N_2(a') \rightarrow e + N_2(X) + N_2^+$	$0.5 \times 2.0 \times 10^{-16}$	[32, 33, 53]
(R16)	$N_2(a') + N(^2P) \rightarrow e + N_3^+$	1.0×10^{-17}	[50]



Table 1 continued

No.	Reaction	Rate coefficient [m ³ /s or m ⁶ /s (*)]	References
(R17)	$N(^2P) + N(^2D) \rightarrow e + N_2^+$	$3.2 \times 10^{-21} T_g^{0.98} / [1 - \exp(-3129/T_g)]$	[50]
(R18)	$N(^2P) + N(^2P) \rightarrow e + N_2^+$	$1.92 \times 10^{-21} T_g^{0.98} / [1 - \exp(-3129/T_g)]$	[50]
<i>Electron-ion recombination</i>			
(R19)	$e + N_2^+ \rightarrow N(^4S) + [0.143 \times N(^4S) + 0.771 \times N(^2D) + 0.086 \times N(^2P)]$	$(1.6-2.2) \times 10^{-13} (300/T_e)^{0.39}$	[29, 50]
(R20)	$e + N_3^+ \rightarrow N_2(X, v) + N(^4S)$	$2.0 \times 10^{-13} (300/T_e)^{0.5}$	[25]
(R21)	$e + N_4^+ \rightarrow N_2(X, v) + N_2(C)$	$2.0 \times 10^{-12} (300/T_e)^{0.5}$	[32, 54]
(R22)	$e + e + N_2^+ \rightarrow e + N_2(X, v)$	$1.0 \times 10^{-31} (300/T_e)^{4.5} (*)$	[32]
(R23)	$e + e + N^+ \rightarrow e + N(^4S)$	$2.0 \times 10^{-39} (10^4/T_e)^{6.04} (*)$	[55]
(R24)	$N^+ + N_2(X) + e \rightarrow N(^4S) + N_2(X)$	$6.07 \times 10^{-34} T_e^{-2.5} (*)$	[56]
<i>Ion conversion</i>			
(R25)	$N_4^+ + N_2(X) \rightarrow N_2^+ + N_2(X) + N_2(X)$	$8.1 \times 10^{-17} \exp[-4842/(T_g + T_v)]$	[25]
(R26)	$N_2^+ + N_2(X) + N_2(X) \rightarrow N_4^+ + N_2(X)$	$5.2 \times 10^{-41} (300/T_g)^{2.2} (*)$	[25]
(R27)	$N_2^+ + N(^4S) \rightarrow N^+ + N_2(X)$	$7.2 \times 10^{-19} (T_g/300)$	[25]
(R28)	$N^+ + N_2(X) \rightarrow N_2^+ + N(^4S)$	1.0×10^{-18}	[25]
(R29)	$N^+ + N_2(X) + N_2(X) \rightarrow N_3^+ + N_2(X)$	$1.7 \times 10^{-41} (300/T_g)^{2.1} (*)$	[25]
(R30)	$N_3^+ + N_2(X) \rightarrow N^+ + N_2(X) + N_2(X)$	$6.0 \times 10^{-16} \exp[-17,000/(T_g + T_v)]$	[25]
(R31)	$N_2^+ + N_2(A) \rightarrow N_3^+ + N(^4S)$	3.0×10^{-16}	[25]
(R32)	$N_3^+ + N(^4S) \rightarrow N_2^+ + N_2(X)$	6.6×10^{-17}	[25]
(R33)	$N_4^+ + N(^4S) \rightarrow N^+ + N_2(X) + N_2(X)$	1.0×10^{-17}	[25]
(R34)	$N_4^+ + N(^4S) \rightarrow N_3^+ + N_2(X)$	1.0×10^{-15}	[25]
<i>Reactions involving electronically excited molecules and atoms</i>			
(R35)	$N_2(A) + N_2(A) \rightarrow N_2(X) + N_2(B)$	3.0×10^{-16}	[57, 58]
(R36)	$N_2(A) + N_2(A) \rightarrow N_2(X) + N_2(C)$	1.6×10^{-16}	[59]
(R37)	$N_2(A) + N_2(X) \rightarrow N_2(X) + N_2(X)$	3.0×10^{-24}	[60]
(R38)	$N_2(A) + N(^4S) \rightarrow N_2(X) + N(^2P)$	$(4.0 \pm 0.5) \times 10^{-17} (300/T_g)^{2.3}$	[61, 62]
(R39)	$N_2(B) + N_2(X) \rightarrow N_2(A) + N_2(X)$	3.0×10^{-17}	[57]

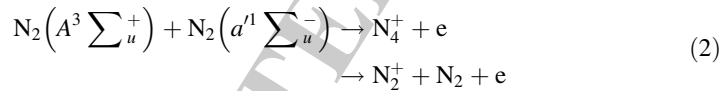


Table 1 continued

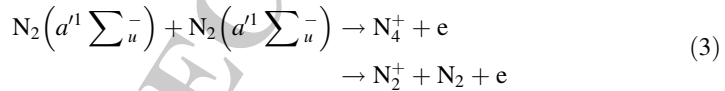
No.	Reaction	Rate coefficient [m ³ /s or m ⁶ /s (*)]	References
(R40)	$N_2(B) + N_2(X) \rightarrow N_2(X) + N_2(X)$	2.0×10^{-18}	[57, 63]
(R41)	$N_2(B) \rightarrow N_2(A) + h\nu$	$1.5 \times 10^5 \text{ s}^{-1}$	[32]
(R42)	$N_2(C) \rightarrow N_2(B) + h\nu$	$3.0 \times 10^7 \text{ s}^{-1}$	[32]
(R43)	$N_2(C) + N_2(X) \rightarrow N_2(d') + N_2(X)$	1.0×10^{-17}	[50]
(R44)	$N_2(d') + N_2(X) \rightarrow N_2(B) + N_2(X)$	$(1.9 \pm 0.5) \times 10^{-19}$	[64]
(R45)	$N(^2P) + N_2(X) \rightarrow N_2(X) + N(^4S)$	6.0×10^{-20}	[30, 34]
(R46)	$N(^2P) + N_2(X) \rightarrow N_2(X) + N(^2D)$	2.0×10^{-24}	[32, 50]
(R47)	$N(^2D) + N_2(X) \rightarrow N_2(X) + N(^4S)$	6.0×10^{-21}	[32, 50]
(R48)	$N(^4S) + N(^4S) + N_2(X) \rightarrow N_2(A) + N_2(X)$	$8.3 \times 10^{-46} \exp(500/T_e) (*)$	[32]
(R49)	$N_2(X, v \geq 11) + N_2(X, v \geq 11) \rightarrow N_2(A) + N_2(X)$	1.0×10^{-22}	[65]
(R50)	$N_2(X, v \geq 16) + N_2(X, v \geq 16) \rightarrow N_2(d') + N_2(X)$	$2.1 \times 10^{-20} \exp(-700/T_e)$	[66]
<i>Thermal dissociation/three body recombination</i>			
(R51)	$N_2(X) + N_2(X) \rightarrow N_2(X) + N(^4S) + N(^4S)$	$4.98 \times 10^{-9} T_e^{-1.5} \exp(-113,260/T_e)$	[56]
(R52)	$N_2(X) + N(^4S) + N(^4S) \rightarrow N_2(X) + N_2(X)$	$4.98 \times 10^{-9} T_e^{-1.5} \exp(-113,260/T_e) K_{52}(T_e)$ (calculated using the principle of detailed balance; see text)	[56]

163 $T_g \sim 4000$ K D is about 1×10^{-3} m²/s. For the conditions of [24] the discharge radius is
 164 $R \approx 1.4$ mm. It follows that the time scales of diffusive losses for charged and neutral
 165 species are about 7×10^{-4} and 2×10^{-3} s; respectively. Such a diffusion time values can
 166 be compared with the corresponding time scale to achieve local equilibrium. For instance,
 167 the time scale for loss of electrons by volume electron-ion recombination (estimated as
 168 $(\beta N_e)^{-1}$, where $\beta = 1.8 \times 10^{-13} (300/T_e)^{0.39}$ m³/s [29]) is about 1×10^{-5} s for an
 169 electron density $N_e \sim 10^{18}$ m⁻³. The time scale for deactivation of $N(^2P)$ by collisions
 170 with $N_2(X)$, whose rate coefficient is $k(N(^2P) - N_2) = 6.0 \times 10^{-20}$ m³/s [30] may be
 171 estimated as $(k(N(^2P) - N_2) N_2(X))^{-1}$. It results 8×10^{-6} s for the conditions of [24]. It
 172 follows that the diffusion losses plays only a minor role in the experimental conditions
 173 analyzed in this work and can be neglected. Also, for conditions as in [24], the motion of
 174 the gas has no appreciable effect on the discharge characteristics, since the influence of a
 175 longitudinal flow at velocities less than 50 cm s⁻¹ is rather weak [31].

176 The model takes into consideration 52 elementary reactions that influence gas heating,
 177 excitation and de-excitation of vibrational and electronic states of nitrogen, dissociation
 178 due to electron and heavy particle impact, generation and loss of the charged particles due
 179 to direct, stepwise and Penning/associative ionization; and volume electron-ion recombina-
 180 tion. The complete set of these processes is summarized in Table 1 (T_g and T_e units are
 181 in K). The rates for almost all processes are known in the literature and are widely used for
 182 nitrogen non-equilibrium discharge modelling (see, for instance, [25, 32]). However, the
 183 ionization reactions



185 and



187 according to reactions (R12)–(R15) in Table 1, have been considered as Penning [33] or
 188 associative [32] ionization (i.e., producing $N_2^+ + N_2 + e$ or $N_4^+ + e$, respectively) owing
 189 to the lack of experimental data. In the present calculation a branching ratio of 0.5 for each
 190 of the two possible products of ionization via (2) and (3) was assumed. The same
 191 assumption was taken in [34].

192 The model approximation for the vibrational energy distribution function (VEDF) for
 193 $N_2(X^1 \sum_g^+, v)$ was assumed as in [25]. The VEDF was divided into three groups. The first
 194 vibrational levels ($v \leq v_1$) closely follow a Boltzmann distribution with temperature T_v
 195 [17]. For the middle vibrational levels ($v_1 < v \leq v_2$) it was assumed the existence of a
 196 ‘plateau’ where $f(v) \sim 1/(v + 1)$; where v_1 and v_2 are the left and right boundaries of the
 197 plateau. After the plateau ($v > v_2$) there is a sharp slope in the VEDF due to fast V–T
 198 relaxation from high-vibrational levels. This slope is characterized by a Boltzmann dis-
 199 tribution with temperature T_g . The width of the plateau decreases with an increase in the
 200 gas temperature [18]. The dependence of the right boundary of the plateau on the gas
 201 temperature was denoted as $v_2 \sim \exp(-(T_g - 300)/3000)$ [25]. Hence, the VEDF was
 202 finally written as:



$$\left. \begin{aligned} N_2(X, v) &= N_2(X, v=0) \exp\left(-v \frac{\hbar\omega}{kT_v}\right), & 0 < v \leq v_1; \\ N_2(X, v) &= N_2(X, v=v_1) \frac{v_1+1}{v+1}, & v_1 < v \leq v_2; \\ N_2(X, v) &= N_2(X, v=v_2) \exp\left(-\frac{\hbar\omega}{kT_g}(v-v_2)\right), & v > v_2; \\ v_1 &= 9, & v_2 &= v_1 + (35 - v_1) \exp\left(-\frac{T_g - 300}{3000}\right); \end{aligned} \right\} \quad (4)$$

where k is the Boltzmann constant and $\nabla\omega$ is the vibrational quantum ($=0.29$ eV) for the nitrogen molecule. Note that the harmonic oscillator model was employed in (4).

The calculation of the rate coefficients for electron-impact excitation (R1)–(R6), dissociation (R7) and ionization (R8); was based on finding the EEDF by means of a solution of the electron Boltzmann equation in the classical two-term approximation with the BOLSIG+ code [35]. The corresponding cross sections were taken from [36]. The effect of the superelastic collisions with vibrationally excited molecules on the processes with high energy threshold (electronic excitation, dissociation and ionization) was accounted for in the BOLSIG+ code by setting the excitation temperature as T_v and the transition energy as the first vibrational threshold (0.29 eV) when solving the Boltzmann equation. Note that the BOLSIG+ code solves the electron Boltzmann equation in a homogeneous electric field within uniform and steady conditions. This assumption is valid as long as the relaxation time for achieving a steady state EEDF is short compared with the characteristic time of discharge development, and the length of the electron energy relaxation is much smaller than the effective discharge radius. Under the present conditions the EEDF relaxation time is $\nu_a^{-1} \sim 10^{-9}$ s (e.g., [18], figure 4.1), which is much smaller than the integration time of (1) to achieve steady conditions ($\sim 10^{-3}$ s). Furthermore, the length of electron energy relaxation is much smaller than the effective discharge radius under conditions typical of molecular plasmas at atmospheric pressure (e.g., [31]). This means that the EEDF is governed by local values of the reduced electric field E/N , the mixture composition, and the vibrational temperature T_v ; which characterizes the first vibrational levels of the VEDF.

The conditions of vibrational excitation also facilitate the dissociation of the nitrogen. The dependence of the rate of the reaction (R51) (thermal dissociation of $N_2(X^1\Sigma_g^+, v)$) on T_v was taken into account through the Macheret–Fridman model [37–39]

$$\begin{aligned} Z(T_g, T_v) &= \frac{1 - \exp\left(-\frac{3354}{T_v}\right)}{1 - \exp\left(-\frac{3354}{T_g}\right)} (1 - L) \exp\left(-113200\left(\frac{1}{T_v} - \frac{1}{T_g}\right)\right) \\ &+ L \exp\left(-113200\left(\frac{1}{T_a} - \frac{1}{T_g}\right)\right); T_a = \alpha T_v + (1 - \alpha) T_g; \quad (5) \\ L &= \frac{2(1 - \alpha)}{\pi^2 \alpha^{3/4}} \left(\frac{T_g}{113200}\right)^{3/2-n} \left(1 + \frac{7(1 - \alpha)(1 + \sqrt{\alpha}) T_g}{2 \times 113200}\right) \end{aligned}$$

where $\alpha = (m_A/(m_A + m_B))^2$ (m_A is the mass of an atom in the dissociating molecule and m_B is the mass of an atom in the impinging molecule) ($=0.25$) for the reaction (R51) and n ($=-1.5$) is the exponent for the temperature T_g in the pre-exponential factor of the Arrhenius form for the rate coefficient of the process (R51). Such a model was found to be the most accurate for nitrogen dissociation under non-equilibrium conditions in a recent study [40].



236 The rate coefficient of the three-body reaction (R52) (the inverse of the thermal dis-
 237 sociation process) was calculated by using the principle of detailed balance; being the
 238 corresponding equilibrium constant $K_{52}(T_g) \equiv [N_2(X)]/([N(^4S)] [N(^4S)])$. The partition
 239 function of the molecules for non-equilibrium conditions was calculated according to the
 240 method proposed in [41] using the molecular parameters taken from [42]. The atomic
 241 partition function was calculated by using the simplified approach presented in [43].

242 The rate coefficients for stepwise ionization from $N_2(A^3\Sigma_u^+)$, $N_2(B^3\Pi_g)$ and $N_2(a^1\Sigma_u^-)$
 243 (R9)–(R11) have been calculated from the cross section data reported in [44] by using the
 244 EEDF calculated with the help of BOLSIG+. The electronic excitation by electron impact
 245 was assumed to occur only from the vibrational ground state $N_2(X^1\Sigma_g^+, 0)$ (the rate
 246 coefficients for electronic excitation, dissociation and ionization from $N_2(X^1\Sigma_g^+, v)$ were
 247 assumed to be the same as those from $N_2(X^1\Sigma_g^+, 0)$) [17].

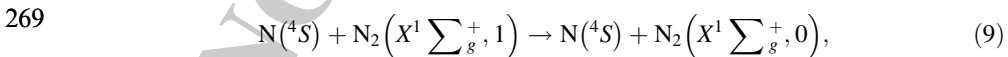
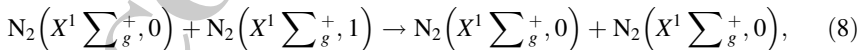
248 The mean-vibrational energy ε_v of the $N_2(X^1\Sigma_g^+, v)$ molecule was described by the
 249 energy balance equation

$$\frac{\partial}{\partial t} (N_2(X)\varepsilon_v) = \eta_v \sigma E^2 - N_2(X) \frac{\varepsilon_v - \varepsilon_v(T_g)}{\tau_{VT}} - 2 \times Q_D, \quad (6)$$

251 where η_v is the fraction of the energy input transferred to the vibrational excitation of
 252 $N_2(X^1\Sigma_g^+, v)$ and σ is the electrical conductivity of the plasma. The mean vibrational
 253 energy of the nitrogen molecule was related to T_v as $\varepsilon_v = \nabla\omega/[\exp(\nabla\omega/(kT_v)) - 1]$; being
 254 $\varepsilon_v(T_g)$ its equilibrium value. τ_{VT} is the time scale of the V–T energy relaxation by
 255 molecules and atoms collisions. At values of the reduced electric field $E/N = 25\text{--}35$ Td,
 256 realized in conditions similar to that of experiment [24], η_v may be estimated with the help
 257 of the BOLSIG+ code as ~ 0.97 (e.g., [16], figure 5.11). A similar approach was used in
 258 [25, 45]. As the BOLSIG+ code only considers excitation reactions of the first vibrational
 259 levels ($v \leq 8$), it might result in underestimated values of this parameter. However, under
 260 the conditions of [24] it is expected that the excitation reactions with $v > 8$ play only a
 261 minor role [17]. The term $2 Q_D$ accounts for the rate of vibrational energy loss due to the
 262 loss of oscillators during strong vibrational non-equilibrium

$$Q_D = \varepsilon_D \left(Z(T_g, T_v) k_{51} N_2 \left(X^1 \Sigma_g^+, v \right)^2 - k_{52} N_2 \left(X^1 \Sigma_g^+, v \right) N \left(^4S \right)^2 \right), \quad (7)$$

264 where $\varepsilon_D \sim 9.76$ eV is the dissociation energy of the nitrogen molecule. Half of this
 265 energy relaxes into kinetic energy [38]. The calculation of τ_{VT} included collisions with
 266 vibrational ground state molecules as well as with dissociated ground state atoms, in
 267 according to the following processes



271 being the corresponding rate coefficients [18]

$$k_{N_2}^{10} (\text{m}^3/\text{s}) = 7.8 \times 10^{-18} T_g \exp \left[-\frac{218}{T_g^{1/3}} + \frac{690}{T_g} \right] \left(1 - \exp \left(-\frac{\hbar\omega}{kT_g} \right) \right)^{-1}, \quad (10)$$

273 and



$$k_N^{10} (\text{m}^3/\text{s}) = 2.3 \times 10^{-19} \exp\left[-\frac{1280}{T_g}\right] + 2.7 \times 10^{-17} \exp\left[-\frac{10840}{T_g}\right]. \quad (11)$$

275 The time scale of the V–T energy relaxation was calculated as [18]

$$\tau_{VT} = \left[\left(1 - \exp\left[-\frac{\hbar\omega}{kT_g}\right] \right) \left(k_{N_2}^{10} N_2(X, 0) + k_N^{10} N(^4S) \right) \right]^{-1}. \quad (12)$$

277 For the conditions of [24] the diffusion time of the nitrogen molecule is about
 279 2×10^{-3} s; which is significantly larger than the V–T relaxation time ($\sim 100 \mu\text{s}$) under
 280 the considered conditions. That is, all the vibrational-excited molecules transform energy
 281 into heat within the discharge zone. The translational temperature of the gas was described
 282 by the equation

$$\frac{\partial}{\partial t} \left(N_2(X) C_p^* T_g \right) = Q_R + Q_D + N_2(X) \frac{\varepsilon_v - \varepsilon_v(T_g)}{\tau_{VT}} - \lambda^* \frac{(T_g - T_\infty)}{R_{th}^2}, \quad (13)$$

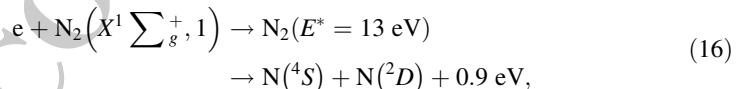
284 where C_p^* is the heat capacity at constant pressure per molecule, Q_R is the ‘fast’ gas heating
 285 rate term, λ^* is the gas thermal conductivity, T_∞ is the ambient gas temperature ($=300$ K)
 286 and R_{th} is the radial length-scale for the variation of T_g . The material quantities C_p^* and λ^*
 287 were calculated by subtracting from the equilibrium values C_p and λ values (taken from
 288 [46]), the contributions related to the vibrational excitation of the nitrogen molecules [31]

$$C_p^* = C_p m_{N_2} - \frac{d\varepsilon_v(T_g)}{dT_g}, \quad (14)$$

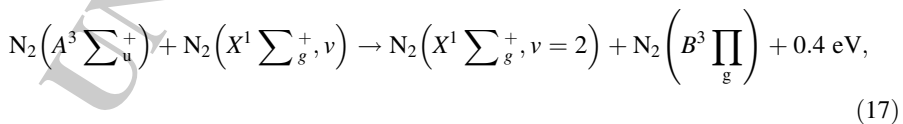
$$\lambda^* = \lambda - N_2(X) D_v \frac{d\varepsilon_v(T_g)}{dT_g}, \quad (15)$$

292 where m_{N_2} is the mass of the nitrogen molecule and D_v its diffusion coefficient. The radial
 293 length-scale for the T_g variation was taken as $R_{th} \sim 2R$, since emission measurements in a
 294 similar experimental conditions [23] than those in [24], indicate that the rotational tem-
 295 perature profile is significantly wider than the charged species concentration profiles. The
 296 same result is shown in a 2-D model of an atmospheric pressure glow discharge [45].

297 The term Q_R accounts for the heat released from chemical reactions in nitrogen gas, as
 298 was described in the model [47]. It included the dissociation reaction (R7) following pre-
 299 dissociation via electronically excited states [47–49]

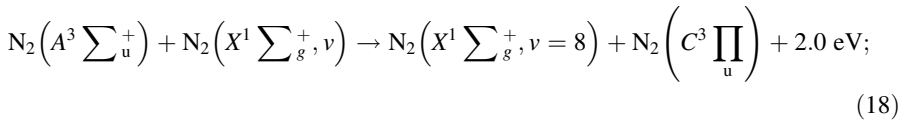


301 the quenching of the electronically excited $N_2(A^3 \sum_u^+)$ states in reaction (R35) [47–49]

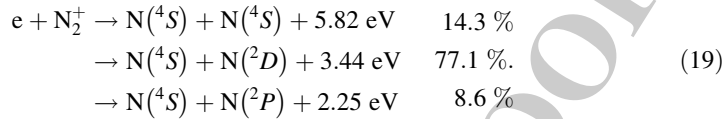




303 and (R36) [47–49]



305 and during the electron-ion recombination processes (R19) [47–50]



307 Thus, the energy which goes to gas heating due to reactions (R19) results 3.7 eV. The
309 fast gas heating term also included the heating at fast translational–translational T–T
310 relaxation (due to the transfer of energy from electrons to molecules in elastic collisions) in
311 according to the reaction (R1); as well as the rotational–translational R–T relaxation of the
312 nitrogen molecule in according to (R2).

313 An estimation of an effective electron temperature T_e as two-thirds of the mean-electron
314 energy was obtained by means of the BOLSIG+ code. The electric field strength was
315 obtained from the Ohm's law [46] for a given value of the discharge current density J and
316 the plasma composition

$$J = \frac{N_e e^2}{\sqrt{2\pi T_e m_e} N Q_{e-n}} E, \quad (20)$$

318 where m_e is the mass of electrons and Q_{en} is the average momentum transfer cross-section
319 for electron-nitrogen collisions. For $T_e \sim 9500$ K, an average momentum transfer cross-
320 section $Q_{e-n} = 1.08 \pm 0.05 \times 10^{-19} \text{ m}^2$ was used [51]. Owing to the low-ionization
321 degree of the discharge ($\delta 10^{-5}$) in the conditions of [24], the average collision frequency
322 between electrons and heavy particles was dominated by collisions with neutrals. During
323 the calculations the consistency of the approximate expression for the electron drift
324 velocity employed in (20) was checked by replacing it by the calculated one on the basis of
325 the EEDF by the BOLSIG+ code. No large differences in the model results were
326 obtained.

327 The input parameter of the model was the discharge current density J inferred from the
328 experimental data of [24]. Initial conditions for all the plasma quantities were used to start
329 the solution procedure ($N_e = N_2^+ \sim 10^{17} \text{ m}^{-3} \gg N_+, N_3^+, N_4^+; N_2(X) = p/(k T_g) -$
330 $N_2(A), N_2(B), N_2(C), N_2(d'), N(^4S), N(^2D), N(^2P);$ being $T_g = T_v \sim 3000$ K and
331 $T_e \sim 9000$ K). The specific values used for these initial conditions did not impact on the
332 final converged results. From a given value of J and the initial plasma composition the
333 electric field strength was calculated from de Ohm's law. Once that the EEDF was found
334 with the help of the BOLSIG+ (from the values of E/N and T_v), the rate coefficients for the
335 process involving electrons (and also the effective electron temperature) were obtained.
336 Then, the continuity equations for atoms ($N(^2D), N(^2P)$ and $N(^4S)$) and the other different
337 charged (N_4^+, N_3^+, N^+ and electrons) and excited species ($N_2(A^3 \sum_u^+), N_2(B^3 \Pi_g), N_2-$
338 $(a^1 \sum_u^-)$ and $N_2(C^3 \Pi_u)$) and the gas thermal and vibrational balance equations were solved
339 to obtain new values of those quantities. Note that in these calculations the charged particle
340 concentrations were constrained through the plasma quasi-neutrality condition. This cal-
341 culation provided new values for the N_2^+ density. The new values for the $N_2(X^1 \sum_g^+,$

342 ν) density were obtained from the constancy of the pressure. The last obtained values of all
 343 the plasma quantities were then taken as new initial values for the next iteration. The
 344 iteration procedure continued until the equilibrium values were reached.

345 The continuity Eq. (1) for the plasma species are quite stiff, i.e., there is a wide range of
 346 time scales associated with the equations, which reduces the time step needed for accurate
 347 numerical integration. This arises because of the wide range of densities and corresponding
 348 source terms for the various species, typically amounting to ten orders of magnitude. The
 349 balance equations were solved numerically by a finite-difference explicit method with the
 350 second-order approximation in time. Because of the stiffness of the equations, a short time-
 351 step for integration ($=1.0 \times 10^{-10}$ s) was used. The Eq. (1) were integrated for times of
 352 $\sim 10^{-3}$ s, and it was sufficient for the density of each species to converge within an error
 353 of about 10^{-3} to its equilibrium value.

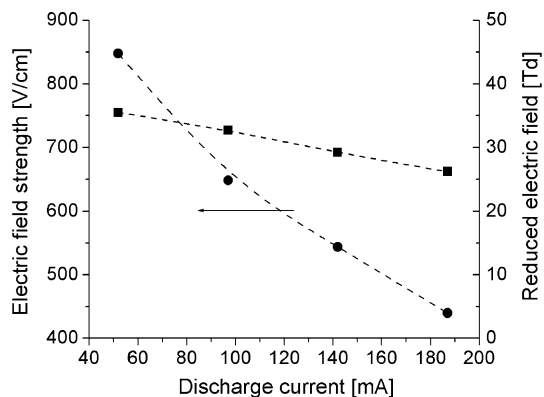
354 Results of Calculations and Discussion

355 The model calculations correspond to the experimental conditions of [24]; where as quoted
 356 previously, the radial profile of the N_2^+ concentration and the values of the gas rotational
 357 temperature were experimentally inferred for currents $I = 52, 97, 142$ and 187 mA. In
 358 order to make comparisons with the model results, the current density at the center
 359 $J(r = 0)$, was determined by dividing the measured current by the effective discharge area
 360 A^* ; i.e., $J(r = 0) \equiv I/A^*$; namely [23, 24]

$$J(r = 0)A^* \equiv 2\pi \int_0^R J(r)rdr, \quad (21)$$

362 being r the radial distance measured from the center of the discharge. As the rotational
 363 temperature profile is significantly wider than the charged species concentration profiles
 364 [23], the local current density $J(r)$ is approximately proportional to the electron density
 365 profile [23, 24]. By assuming that the electron density is proportional to the measured N_2^+
 366 at each radial position [24]; A^* was calculated as

Fig. 1 Electric field strength and reduced electric field versus the discharge current



$$A^* \equiv \frac{2\pi}{N_2^+(r=0)} \int_0^R N_2^+(r) r dr. \quad (22)$$

Thus Eq. (22) was employed to derive the current density at the center of the discharge column by using the measured radial profiles of N_2^+ ([24], figure 5) for each current value. The calculated values of $J(r=0)$ for $I = 52, 97, 142$ and 187 mA, were $\sim 0.8, 1.6, 2.2$ and 3 A/cm²; respectively. The electric field strength together with the plasma composition and the electron and gas temperature, as well as the vibrational temperature characterizing the first vibrational levels of the nitrogen ground state molecules were calculated from these values of current density. As a consequence, the model output gives estimations of the discharge variables evaluated at the center of the discharge under the experimental conditions of [24].

Figure 1 shows the values of the electric field and also the reduced electric field versus the discharge current. The electric field decreases when the current increases, resulting in a negative slope in the E - I characteristic of the discharge. A similar trend is observed for the reduced electric field. This behavior was observed in several works for this kind of discharge [4, 5, 7].

Figure 2 shows the values of the electron temperature, the gas temperature and the vibrational temperature of the nitrogen molecules versus the discharge current. As it can be seen, the vibrational temperature values are higher than the gas temperature in the given current range (thus indicating that the nitrogen molecules are in vibrational non-equilibrium state) being its difference smaller as the discharge current increases. This is expected since the rate of V-T energy transfer (12) and (13) increases exponentially with T_g . A noticeable difference between the T_e and T_g values is also observed. The T_e values (~ 9500 K) are typical of this kind of low-current discharges in molecular gases [31, 45]. As it can be seen, as the discharge current increases the electron temperature softly decreases while the gas temperature increases (with rather high values, above 3000 K); and consequently the plasma non-equilibrium degree decreases; but it is still maintained at a relatively high level $T_e/T_g \approx 2$. The calculated gas temperature values show good agreement with the experimental data [24] (within the experimental error of $\pm 8\%$) in the whole current range.

Fig. 2 The electron, vibrational and gas temperatures versus the discharge current

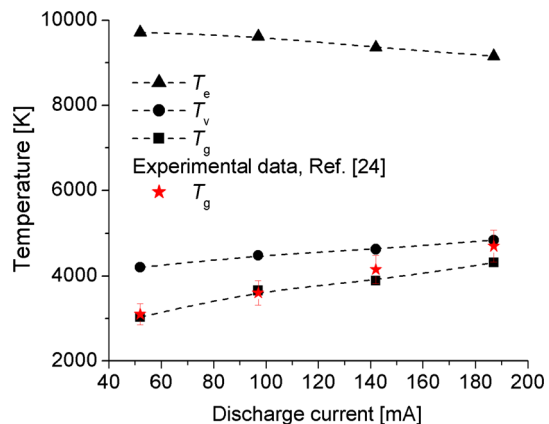
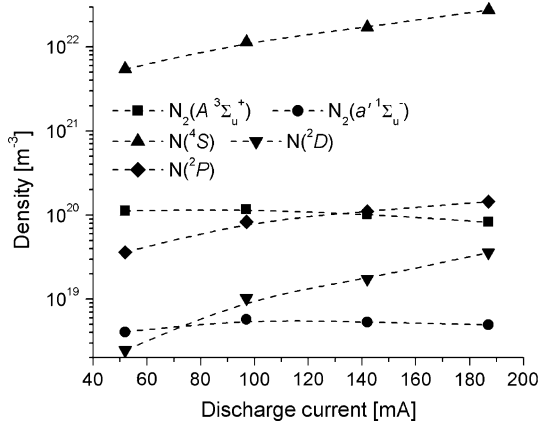


Fig. 3 Densities of the electronic molecular and atomic metastable states and the electronic atomic ground state versus the discharge current



396 Figure 3 shows the densities of the electronic molecular and atomic metastable states
 397 and the electronic atomic ground state versus the discharge current. The rather high-gas
 398 temperature together with the vibrational non-equilibrium leads to the production of dis-
 399 sociation products as $N(4S)$, $N(2D)$ and $N(2P)$; mainly due to non-equilibrium thermal
 400 dissociation (see Fig. 4). The nitrogen dissociation degree varies in the range ~ 0.2 to
 401 1.6 % in the whole current range. About 99 % of the atoms are in the ground state. The
 402 density of $N(2P)$ is higher than that of $N(2D)$ due to the production of the $N(2P)$ by the
 403 quenching of the $N_2(A^3\Sigma_u^+)$ states through the reaction (R38) (see Fig. 5); thus producing
 404 a decrease in the density of the molecular metastable $N_2(A^3\Sigma_u^+)$ and an increase in the
 405 density of $N(2P)$ as the discharge current increases. An increase in the density of the $N(2D)$
 406 state for the larger values of the discharge current is also observed because the $N(2D)$
 407 is mainly created by dissociative recombination (R19) in Table 1. The density of $N_2(a'1\Sigma_g^-)$
 408 is lower than that of $N(2D)$ almost in the whole current range (except for the smaller values
 409 of the discharge current).

410 Figure 4 shows a comparison between the electron-impact dissociation (R7) in Table 1
 411 with the thermal dissociation for vibrational excited molecules, accounted for by using the
 412 multiplicative non-equilibrium factor (5) in the rate coefficient of the reaction (R51) in

Fig. 4 Dissociation contributions versus the discharge current

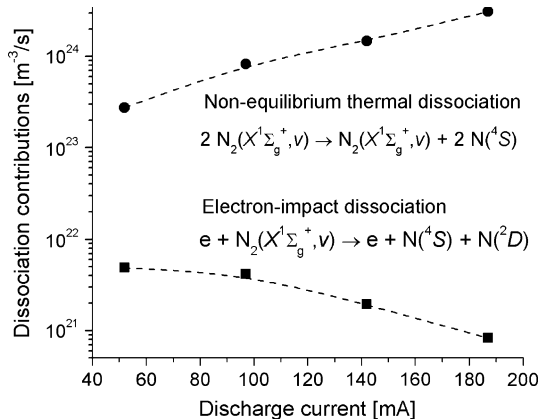
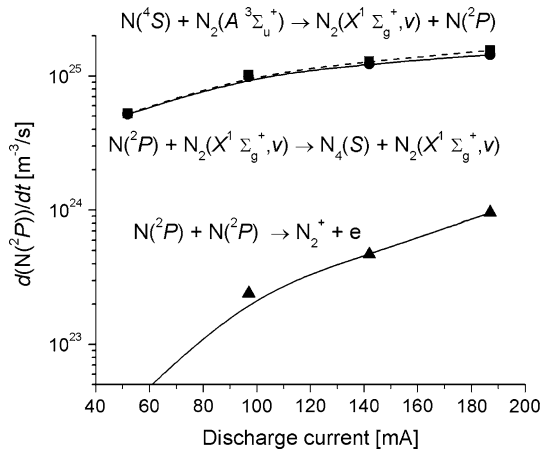
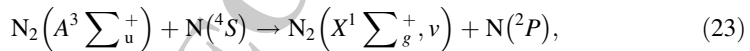


Fig. 5 Rates of the atomic metastable $N(^2P)$ production and loss via different mechanisms versus the discharge current



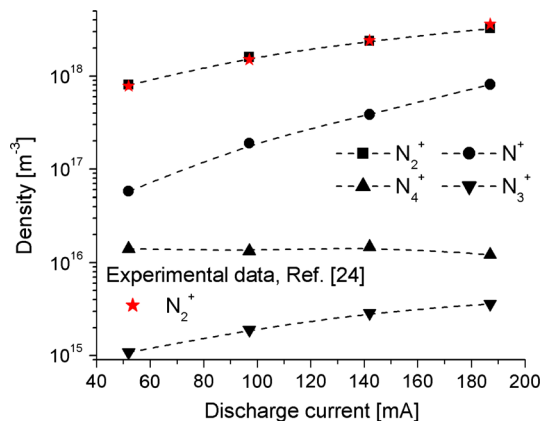
413 Table 1. As it can be seen, several orders of magnitude exist between both dissociation
 414 rates; thus suggesting that the electron-impact dissociation process is not important under
 415 the considered low-electric field conditions; but the thermal dissociation of vibrationally
 416 excited molecules plays an essential role in the production of $N(^4S)$ atoms. It should be
 417 noted that the used Macheret–Fridman model imposes no restriction onto the values of T_g
 418 and T_v , and does not depend on any semi-empirical parameter [37, 38].

419 Figure 5 shows the rates of the atomic metastable $N(^2P)$ production and loss via dif-
 420 ferent mechanisms versus the discharge current. It is observed that the dominant process of
 421 production of $N(^2P)$ (marked with a dashed line in Fig. 5) within the whole current range is
 422 the quenching of the $N_2(A^3\Sigma_u^+)$ state through the reaction (R38)



424 while the loss is almost due to the quenching of $N(^2P)$ in collisions with $N_2(X^1\Sigma_g^+,$
 425 $v)$ molecules through the reaction (R45) in Table 1; being both processes in a sort of
 426 detailed balance. The low difference between the rates of such processes for the larger

Fig. 6 Ion composition of the plasma versus the discharge current



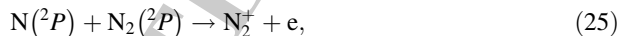
427 current values is due to the increasing importance of the ionization associative process
 428 (R18). Under the analyzed conditions, the excitation rate of the $N_2(A^3\Sigma_u^+)$ state due to
 429 mutual collisions of strongly vibrationally excited molecules in according to the reaction
 430 (R49), is much lower than the excitation rate due to collisions of energetic electrons with
 431 molecules in according to the reaction (R3). That is, the excitation rate of the $N_2(A^3\Sigma_u^+)$
 432 state is determined by the EEDF (calculated by the help of the BOLSIG+ code) and not by
 433 the approximation model of the VEDF.

434 Figure 6 shows the ion composition of the plasma versus the discharge current. As it can
 435 be seen, the dominant ion within the whole current range is the molecular N_2^+ , in
 436 according to experimental data [24]. Approximately 92, 88, 86 and 80 % of the ions are
 437 N_2^+ , the remainder is almost the atomic N^+ . The following inequality holds:

$$N_2^+ + N^+ \gg N_3^+ + N_4^+. \quad (24)$$

440 The results on the plasma composition are quite different from those found in the model
 441 [25] for a current $I = 40$ mA, but the present results show good agreement (within the
 442 experimental error of $\pm 10\%$) with the peak values of the N_2^+ radial profiles measured in
 443 [24] in the whole current range. Note that it is quite irrelevant to consider reactions (R12)–
 444 (R15) as Penning or associative ionization processes, since the density of N_4^+ ions are
 445 quickly converted in N_2^+ due to the ion conversion reactions (R25)–(R34) in Table 1.

446 Figure 7 shows the rate of the electron production and loss via several mechanisms versus
 447 the discharge current. As it can be seen, the dominant process of production of electrons
 448 within the almost whole current range is the associative ionization in atomic collisions



450 in according to the process (R18) in Table 1. Only for low-current values ~ 50 mA or
 451 lower, the rate of the Penning/associative ionization process through reactions (R12) and
 452 (R13) in Table 1,

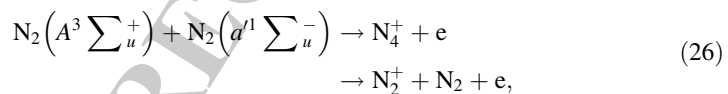


Fig. 7 Rates of the electron production and loss via several mechanisms versus the discharge current

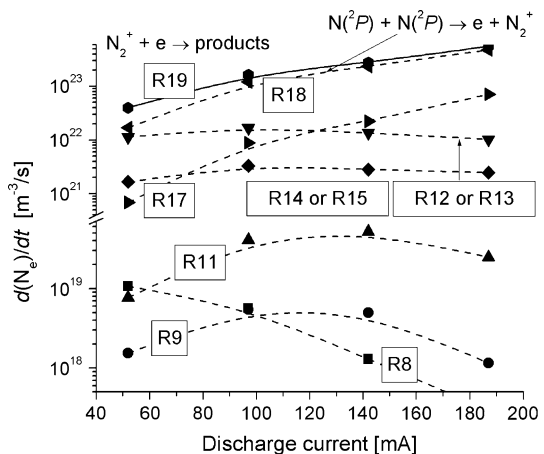
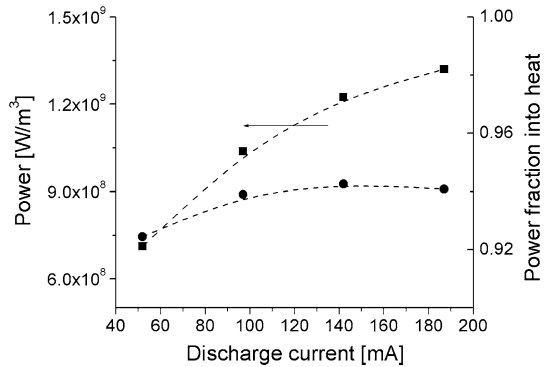


Fig. 8 Electron power and the fraction of it converted into heat versus the discharge current



454 approaches to the rate of the process (R18). This is because the gas temperature is not high
 455 enough; however an increase in the current values (and thus in the gas temperature) leads
 456 to an exponential increase in the rate of the process (R18) until it is balanced with the
 457 dissociative recombination process (R19) (marked with a solid line in Fig. 7). For the
 458 larger current values, also the rate of ionization in according to the process (R17)



460 exceeds the rate of the processes (R12) and (R13) due to the strong increase in the density
 461 of the $N(^2D)$ state (as is shown in Fig. 3). The processes of direct electron-impact ion-
 462 ization (R8) as well as the stepwise ionization from the metastables $N_2(A^3\Sigma_u^+)$, and
 463 $N_2(a^1\Sigma_u^-)$, in according to reactions (R9) and (R11) respectively; are not important under
 464 the present conditions.

465 According to these results, the associative ionization in atomic collisions might plays a
 466 non-negligible role in the production of electrons under the conditions of [25], because the
 467 high-gas temperature ($T_g \sim 3600$ K) predicted by that model at $I = 40$ mA for the
 468 nitrogen gas at rest.

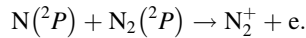
469 Figure 8 shows the electron power and the fraction of it converted into heat versus de
 470 discharge current. As it can be seen, a very large fraction (up to ~ 94 %) of the electron
 471 power is converted into heat. The major source of gas heating is the V–T relaxation of
 472 nitrogen molecules owing to the rather high-gas temperature values of the discharge. The
 473 heat released from chemical reactions does not play any relevant role under these condi-
 474 tions because the fraction of the electron power transferred to the electronic excitation of
 475 the nitrogen is low (< 2 %).

476 Conclusions

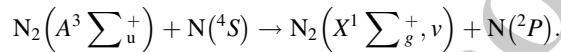
477 A model describing an atmospheric pressure glow discharge in nitrogen gas to simulate the
 478 experimental conditions of [24], accounting for several processes with the participation of
 479 electronically excited atoms, was developed. The basic processes sustaining the discharge
 480 at a current range of 52–187 mA were identified. A good agreement between the calculated
 481 results and the experiment [24] was found. The model has shown that:



- 482 1. The thermal dissociation of vibrationally excited molecules plays an essential role in
 483 the production of $N(^4S)$ atoms. The electron-impact dissociation process is not
 484 important under the considered low-electric field conditions.
- 485 2. The dominant ion within the investigated current range is the molecular N_2^+ with an
 486 increasing proportion of atomic N^+ toward high-current values. The dominant process
 487 of production of electrons within the almost whole current range is the associative
 488 ionization in atomic collisions



- 491
- 490 3. The dominant process of production of $N(^2P)$ within the whole current range is the
 493 quenching of the $N_2(A^3\Sigma_u^+)$ electronically excited molecules by nitrogen atoms



- 496
- 495 4. A very large fraction (up to $\sim 94\%$) of the electron power is converted into heat. The
 498 major source of gas heating is the V–T relaxation of nitrogen molecules owing to the
 499 rather high-gas temperature values of the discharge.

500 **Acknowledgments** This work was supported by Grants from the CONICET (PIP 11220120100453) and
 501 Universidad Tecnológica Nacional (PID 2264). L. P. and H. K. are members of the CONICET.

502

503 References

- 504 1. Park GY, Park SJ, Choi MY, Koo IG, Byun JH, Hong JW, Sim JY, Collins GJ, Lee JK (2012) Plasma
 505 Sources Sci Technol 21:21
- 506 2. Fridman A, Chirokov A (2005) J Phys D Appl Phys 38:R1–R24
- 507 3. Kunhardt EE (2000) IEEE Trans Plasma Sci 28:189–200
- 508 4. Gambling WA, Edels H (1954) Br J Appl Phys 5:36–39
- 509 5. Machala Z, Marode E, Laux CO, Kruger CH (2004) J Adv Oxid Technol 7:133–137
- 510 6. Staack D, Farouk B, Gutsol A, Fridman A (2008) Plasma Sources Sci Technol 17:13
- 511 7. Verreycken T, Schram DC, Leys C, Bruggeman P (2010) Plasma Sources Sci Technol 19:9
- 512 8. Machala Z, Laux CO, Kruger CH (2005) IEEE Trans Plasma Sci 33:320–321
- 513 9. Staack D, Farouk B, Gutsol A, Fridman A (2005) Plasma Sources Sci Technol 14:700–711
- 514 10. Wilson A, Staack D, Farouk T, Gutsol A, Fridman A, Farouk B (2008) Plasma Sources Sci Technol
 515 17:12
- 516 11. Prevosto L, Kelly H, Mancinelli B, Chamorro JC, Cejas E (2015) Phys Plasmas 22:8
- 517 12. Staack D, Farouk B, Gutsol A, Fridman A (2009) J Appl Phys 106:7
- 518 13. Bayle P, Bayle M, Forn G (1985) J Phys D Appl Phys 18:2395–2415
- 519 14. Hsu CC, Wu CY (2009) J Phys D Appl Phys 42:8
- 520 15. Akishev Yu, Goossens O, Callebaut T, Leys C, Napartovich A, Trushkin N (2001) J Phys D Appl Phys
 521 34:2875–2882
- 522 16. Raizer YP (1991) Gas discharge physics. Springer, Berlin
- 523 17. Boeuf JP, Kunhardt EE (1986) J Appl Phys 60:915–923
- 524 18. Capitelli M, Ferreira CM, Gordiets BF, Osipov AI (2000) Plasma kinetics in atmospheric gases.
 525 Springer, New York
- 526 19. Velikhov EP, Golubev VS, Pashkin SV (1982) Sov Phys Usp 25:340–358
- 527 20. Eletskii AV, Smirnov BM (1996) Phys Usp 39:1137–1156
- 528 21. Akishev Y, Grushin M, Karalnik V, Petryakov A, Trushkin N (2010) J Phys D Appl Phys 43:11
- 529 22. Kruger CH, Laux CO, Yu L, Packan DM, Pierrot L (2002) Pure Appl Chem 74:337–347
- 530 23. Yu L, Laux CO, Packan DM, Kruger CH (2002) J Appl Phys 91:2678–2686
- 531 24. Yalin AP, Laux CO, Kruger CH, Zare RN (2003) Plasma Sources Sci Technol 11:248–253
- 532 25. Akishev Y, Grushin M, Karalnik V, Petryakov A, Trushkin N (2010) J Phys D Appl Phys 43:18



- 533 26. Pierrot L, Yu L, Gessman RJ, Laux CO, Kruger CH (1999) In: Proceedings of 30th AIAA plasma-
534 dynamics and lasers conference, AIAA 99-3478, Norfolk, VA
- 535 27. Hugill J, Saktioto T (2001) Plasma Sources Sci Technol 10:38–42
- 536 28. Saporoschenko M (1965) Phys Rev 139:352–356
- 537 29. Mehr FJ, Biondi MA (1969) Phys Rev 181:264–271
- 538 30. Lin CL, Kaufman F (1971) J Chem Phys 55:3760–3770
- 539 31. Naidis GV (2007) Plasma Sources Sci Technol 16:297–303
- 540 32. Kossyi IA, Kostinsky AY, Matveyev AA, Silakov VP (1992) Plasma Sources Sci Technol 1:207–220
- 541 33. Brunet H, RocaSerra J (1985) J Appl Phys 57:1574–1581
- 542 34. Guerra V, Sa PA, Loureiro J (2004) Eur Phys J Appl Phys 28:125–152
- 543 35. Hagelaar GJM, Pitchford LC (2005) Plasma Sources Sci. Technol. 14:722–733; freeware code BOL-
544 SIG+ version 07/2015. www.bolsig.laplace.univ-tlse.fr (2015)
- 545 36. SIGLO database, <http://www.lxcat.laplace.univ-tlse.fr>. Retrieved June 4, 2013
- 546 37. Macheret SO, Rich JW (1993) Chem Phys 174:25–43
- 547 38. Fridman AA, Kennedy LA (2004) Plasma physics and engineering. Taylor & Francis, London
- 548 39. Chernyi GG, Losev SA, Macheret SO, Potapkin BV (2002) Physical and chemical processes in gas
549 dynamics: cross sections and rate constants, vol 1. AIAA, New York
- 550 40. da Silva ML, Guerra V, Loureiro J (2007) Chem Phys 342:275–287
- 551 41. Andre P, Abbaoui M, Lefort A, Parizet MJ (1996) Plasma Chem Plasma Process 16:379–397
- 552 42. Huber KP, Herzberg G (1979) Molecular spectra and molecular structure: IV constants of diatomic
553 molecules. Springer, Berlin
- 554 43. D'Ammando G, Colonna G, Pietanza LD, Capitelli M (2010) Spectrochim Acta Part B 65:603–605
- 555 44. Bacri J, Medani A (1982) Phys C 112:101–118
- 556 45. Benilov MS, Naidis GV (2003) J Phys D Appl Phys 36:1834–1841
- 557 46. Boulou M, Fauchais P, Pfender E (1994) Thermal plasmas, fundamentals and applications, vol 1.
558 Plenum Press, New York and London
- 559 47. Popov NA (2001) Plasma Phys Rep 27:886–896
- 560 48. Popov NA (2011) J Phys D Appl Phys 44:16
- 561 49. Mintousov EI, Pendleton SJ, Gerbault FG, Popov NA, Starikovskaia SM (2011) J Phys D Appl Phys
562 44:13
- 563 50. Matveyev AA, Silakov VP (1999) Plasma Sources Sci Technol 8:162–178
- 564 51. Itikawa Y (2006) J Phys Chem Ref Data 35:31–53
- 565 **AQ2** 52. Aleksandrov NL, Bazelyan EM, Kochetov IV, Dyatko NA (1997) J Phys D Appl Phys 30:1616–1624
- 566 53. Brunet H, Vincent P, RocaSerra J (1983) J Appl Phys 54:4951–4957
- 567 54. Cao YS, Johnsen R (1991) J Chem Phys 95:7356–7359
- 568 55. Bourdon A, Vervisch P (1996) Phys Rev E 54:1888–1898
- 569 56. Dunn MG, Lordi JA (1970) AIAA J. 8:339–345
- 570 57. Piper LG (1988) J Chem Phys 88:6911–6921
- 571 58. Hays GN, Oskam HJ (1973) J Chem Phys 59:1507–1516
- 572 59. Piper LG (1988) J Chem Phys 88:231–232
- 573 60. Clark WG, Setser DW (1980) J Chem Phys 84:2225–2233
- 574 61. Tatarova E, Dias FM, Gordiets B, Ferreira CM (2005) Plasma Sources Sci Technol 14:19–31
- 575 62. Piper LG (1989) J Chem Phys 90:7087–7095
- 576 63. Heidner RF, Sutton DG, Suchard SN (1976) Chem Phys Lett 37:243–248
- 577 64. Piper LG (1987) J Chem Phys 87:1625–1629
- 578 65. Gordiets BF, Ferreira CM, Guerra VL, Loureiro JMAH, Nahorny J, Pagnon D, Touzeau M, Vialle M
579 (1995) IEEE Trans Plasma Sci 23:750–768
- 580 66. Gordiets B, Ferreira CM, Pinheiro MJ, Ricard A (1998) Plasma Sources Sci Technol 7:363–378

Journal : **11090**
Article : **9716**



Author Query Form

**Please ensure you fill out your response to the queries raised below
and return this form along with your corrections**

Dear Author

During the process of typesetting your article, the following queries have arisen. Please check your typeset proof carefully against the queries listed below and mark the necessary changes either directly on the proof/online grid or in the 'Author's response' area provided below

Query	Details Required	Author's Response
AQ1	Kindly check and confirm the inserted initial for the author 'Bruggeman' is correct in reference [7].	
AQ2	Reference [52] was provided in the reference list; however, this was not mentioned or cited in the manuscript. As a rule, if a citation is present in the text, then it should be present in the list. Please provide the location of where to insert the reference citation in the main body text. Kindly ensure that all references are cited in ascending numerical order.	